Bulletin of the JSME Vol.17, No.2, 2022
Journal of Biomechanical Science and Engineering

Development of vibration mechanical stimuli loading device for live cell fluorescence microscopy

Katsuya SATO* and Daiki OOMORI**
*Graduate School of Technology, Industrial and Social Sciences, Tokushima University
2-1 Minami Josanjima, Tokushima 770-8506, Japan
E-mail: katsuyas@tokushima-u.ac.jp
**Graduate School of Advanced Technology and Science, Tokushima University
2-1 Minami Josanjima, Tokushima 770-8506, Japan

Received: 23 August 2021; Revised: 10 November 2021; Accepted: 29 November 2021

Abstract
Bone metabolism is regulated by mechanical stimuli such as gravity and exercise. If bone formation can be promoted by artificial mechanical stimulation, the quality of life of the aging society can be improved, such as by reducing the progression of osteoporosis and preventing patients from being bedridden. Micro-vibration stimulation with frequencies of 15 Hz to 90 Hz and acceleration amplitudes of 0.1 g to 0.3 g is effectively promotes bone formation in animal models. However, the mechanism of how these weak vibrations are sensed by bone cells and are used to regulate bone metabolism is unknown. In this study, we developed a device to apply micro-vibration stimuli to osteoblasts cultured on a glass bottom dish and observed the cell response to the stimuli using a confocal laser scanning fluorescence microscope. The device performance was confirmed using driving tests, and the calcium signaling response of osteoblasts to micro-vibration stimuli was observed in real time and *in situ*. The calcium signaling response characteristics of the cells differed when the cells were subjected to 45 Hz and 90 Hz micro-vibration stimuli, even under a constant acceleration amplitude of 0.2 g.

Keywords : Vibration stimuli, Osteoblast, Calcium signaling, Cell biomechanics, Mechanotransduction

1. Introduction

Osteoporosis is a disease in which bones become brittle with aging because of a decrease in bone mass and density caused by a decrease in calcium and other substances in bone tissue. This disease is more common in the elderly, and the number of patients is expected to increase as the population ages. As osteoporosis progresses, the mechanical properties of bone deteriorate, which can lead to fractures induced by falls and other causes, leading to bedridden patients. Prevention and treatment of osteoporosis is an important public health issue to address the quality of life of the elderly; however, the current situation remains a challenge. Osteoporosis is currently treated by pharmacological methods, the most common being estrogen replacement therapy (Lindsay and Tohme, 1990). However, this therapy has side effects such as breast cancer, endometrial hyperplasia, coronary artery disease, and venous thromboembolism (Levin, et al., 2018). In recent years, alternative non-pharmacological methods, such as physical exercise and strength training, have been introduced and are becoming increasingly important. Artificially controlled mechanical stimulation is expected to increase the therapeutic effect of pharmacological methods and reduce their side effects for the prevention and treatment of osteoporosis.

Animal model experiments have been used to demonstrate that low-magnitude, high-frequency (LMHF) micro-vibration stimulation promotes bone formation in osteoporotic mice and improves the material properties of the trabecular and cortical bone (Hwang, et al., 2008; Leung, et al., 2009; Rubin, et al., 2004; Tezval, et al., 2011). LMHF vibrations have an acceleration amplitude of 0.1 g to 0.3 g and a frequency of 15 Hz to 90 Hz, which are greater than the repetitive strain cycle caused by human walking and locomotion (several Hz), and the magnitude of strain produced in the bone is approximately 1/1000 (several με), which is a very weak mechanical stimulus (Fritton, et al., 2000; Judex, et al., 2007; Xie, et al., 2006). Because the deformation of the bone matrix caused by LMHF vibration is very small, the strain itself

Paper No.21-00294
J-STAGE Advance Publication date : 8 December, 2021
[DOI: 10.1299/jbse.21-00294]

and the shear stress caused by the flow of tissue fluid are also expected to be very small. The mechanism of how osteoblasts and other bone cells sense this micro-vibration stimulus and link it to the activation of osteogenic activity is not clear. In this study, as a first step to elucidate the mechanism osteoblasts detect LMHF vibration, we simplified the experimental system to one that uses cultured cells *in vitro*, and evaluated the response of osteoblasts to LMHF vibration stimuli. The calcium signaling response is upstream of the cellular biochemical signaling cascade, and characteristics, such as the amount, duration, and frequency of transient increases in intracellular calcium ion concentration, are referred to as calcium response fingerprints and regulate various cellular functions (Godin, et al., 2007; Huo, et al., 2008; Lu, et al., 2012). To evaluate these transient calcium signaling response characteristics, which may change in a few seconds or tens of seconds, it is necessary to perform real time *in situ* observation at the single cell level on cells subject to LMHF vibration stimuli. For this purpose, we developed an original device for real time *in situ* observation of the calcium signal response to LMHF vibration stimulation of osteoblasts cultured on a glass bottom dish using a confocal laser scanning fluorescence microscope. The device performance was confirmed through driving tests, and the calcium signaling response of osteoblasts to LMHF vibration stimuli was observed in real time and *in situ*. The calcium signaling response characteristics of the cells were different at 45 Hz and 90 Hz LMHF vibration stimuli.

2. Materials and Methods

2.1 LMHF vibration loading device

Figure 1 is a schematic diagram of the LMHF vibration loading device configuration. The device is placed on the stage of an inverted microscope. The vibration plate is fixed via two linear sliders attached to the base plate, and the vibration plate is connected to the piezoelectric actuator by a connecting jig. A dish holder is installed at the center of the vibration plate, and a glass bottom dish with a diameter of 35 mm is fixed to the dish holder using a urethane sponge. The vibrating plate is reciprocated horizontally by a piezoelectric actuator, and the cells seeded on the glass bottom dish are subject to vibration.

Figure 2 is a photograph of the device placed on the stage of a microscope. The base plate is made of A5052 aluminum alloy, and the vibration plate and dish holder are acrylic to reduce the weight of the vibration part. The piezoelectric actuator (MC-140L, Mess-Tek, Japan) is an elastic hinge mechanism with a pivoting motion and a stroke of 140 μm. The driving voltage signal waveform is sinusoidal, and the voltage signal generated by the Arduino microcomputer and digital analog converter chip (MCP4725 breakout board, Adadruit, USA) is amplified by the piezoelectric amplifier (M-2691, Mess-Tek, Japan) to drive the actuator. The acceleration amplitude was set to 0.2 g and the frequency was set to 45 Hz and 90 Hz. Therefore, the amplitudes of the vibrations at each frequency are approximately 49 μm and 12 μm.

2.2 Cell culture and fluorescent labeling

The mouse osteoblastic cell line MC3T3-E1 was provided by RIKEN BRC through the National Bio-Resource Project of the Ministry of Education, Culture, Sports, Science and Technology, Japan. Cells were pre-cultured in α-minimum essential medium containing 10 % fetal bovine serum and they were maintained at 37 °C with 5 % CO_2. Prior to the experiment, cells were seeded on a fibronectin-coated, 35-mm glass bottom dish at a density of 3×10^4 cells/dish. After 12 hours of incubation for sufficient cell adhesion, fluorescent Ca^{2+} indicator Fluo 8H and fluorescent cell-permeant

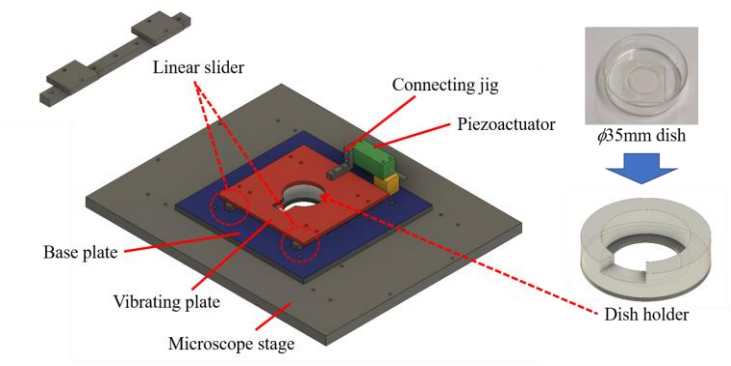

Fig.1 Schematic of vibration loading device

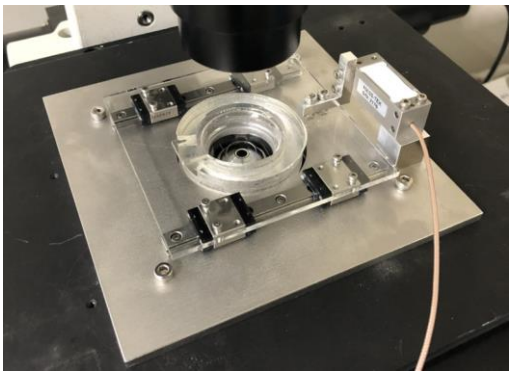

Fig.2 Vibration loading device mounted on the microscope stage

[DOI: 10.1299/jbse.21-00294]

dye Calcein Red-Orange were loaded into the cells. Hank's balanced salt solution (HBSS) containing 12 μM Fluo 8H-AM (AAT bioquest, USA), 5 μM Calcein Red-Orange (Thermo Fisher Scientific, USA), and 0.1 % Pluronic F-127 (Life Technologies, USA) was used as a loading buffer. Fluo 8H increases its fluorescent intensity as the Ca^{2+} concentration increases. Conversely, the fluorescent intensity of Calcein Red-Orange is independent of the Ca^{2+} concentration. The fluorescent intensity of Fluo 8H changes by both the influence of intracellular calcium ion concentration ($[Ca^{2+}]_i$) and motion artifacts during the vibration application. In contrast, the fluorescent intensity of Calcein Red-Orange changes by the influence of motion artifacts only. Therefore, to calculate the ratio of fluorescent intensities (Fluo 8H : Calcein Red-Orange), we evaluated the change in $[Ca^{2+}]_i$ without the influence of motion artifacts. Normal culture medium was replaced with the loading buffer, and the cells were cultured for 30 minutes in the CO_2 incubator to load the fluorescent indicator dyes into the cells. After dye loading, the cells were rinsed twice with Dulbecco's phosphate-buffered saline and used for fluorescence image acquisition in HBSS (recording buffer).

2.3 Imaging system and settings

Confocal laser scanning fluorescence microscopy (A1R, Nikon, Japan) was used for the driving tests and to observe the cell responses. For the driving test, a 20× dry lens was used as the objective lens. The resonant scan mode was used with an imaging resolution of 512 × 32 pixels. The scan rate was 420 frames per second. Only transmitted light was acquired; fluorescence images were not used. A 40× dry lens was used to observe the cell response. The galvano scan mode was used, the image resolution was 512 × 512 pixels, and the scan rate was 1 frame per second. Lasers (488 nm and 561 nm) were used as the excitation light. A bandpass filter with a central wavelength of 525 nm and a bandwidth of 50 nm was used to image the Fluo 8H, and a bandpass filter with a central wavelength of 595 nm and a bandwidth of 50 nm was used to image the Calcein Red-Orange. The fluorescence of the two dyes was simultaneously imaged using independent photomultiplier tubes. The baseline values were acquired without vibration stimulation for 30 seconds after initiating imaging, and vibration stimulation was applied after 30 seconds. The observation time for each experiment was set to 15 minutes to reduce the effect on the cells in normal atmosphere. No changes in cell adhesion or shape were observed after 15 minutes of vibration stimulation in normal atmospheric conditions, suggesting no adverse effects (data not shown).

2.4 Definition of the ROI and image analysis

As shown in Fig.3, because of the image construction principle of the scanning microscope, images of cells subjected to vibration had distortions. Additionally, the shape of the distorted image changed in each time series image. To simplify the measurement of fluorescence intensity by image analysis, the ROI for measuring the average fluorescence intensity was initially set to a fixed shape. Figure 4 shows the fluorescent images of the cells before vibration and the same cells after vibration at 45 Hz and 90 Hz. In this experiment, the intensity of the vibration was maintained at an acceleration amplitude of 0.2 g. Therefore, the amplitudes at 45 Hz and 90 Hz are different (actual vibration amplitude were 49 μm for 45 Hz and 12 μm for 90 Hz) When the cells are surrounded by a simple curve with manual tracing, as shown in Fig.5, the fluorescent part of the cells and the background are mixed in the ROI, and the area of the ROI is the largest at 45 Hz.

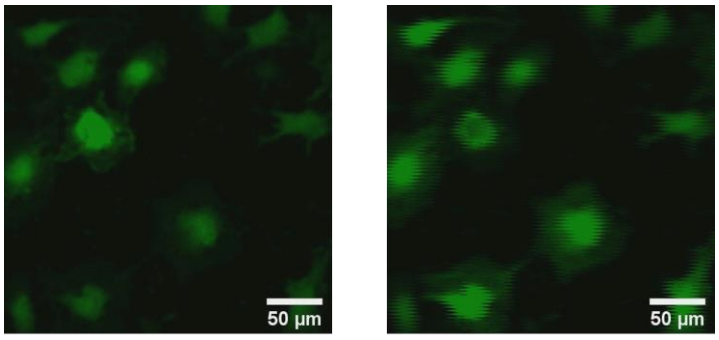

(a) Initial state (b) under vibration

Fig.3 Distortion of confocal microscope images because of the application of vibration

[DOI: 10.1299/jbse.21-00294]

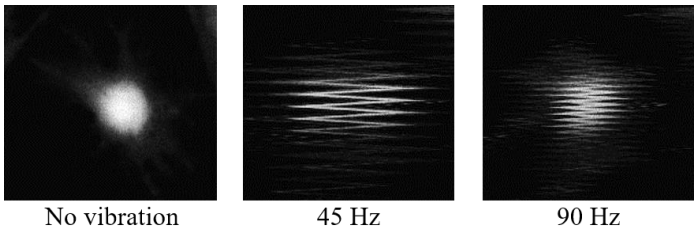

Fig.4 Difference of the distorted images according to the vibration frequency

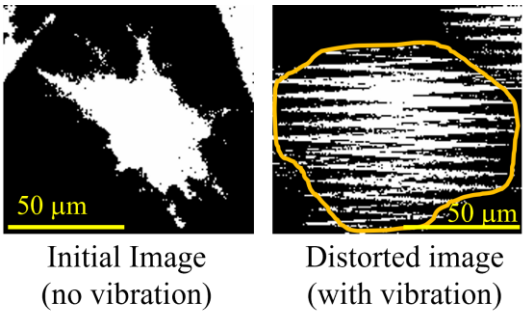

Fig.5 Binarized image of a cell at the initial state and under vibration state. Example of a set ROI to enclose the entire shape, including distortion.

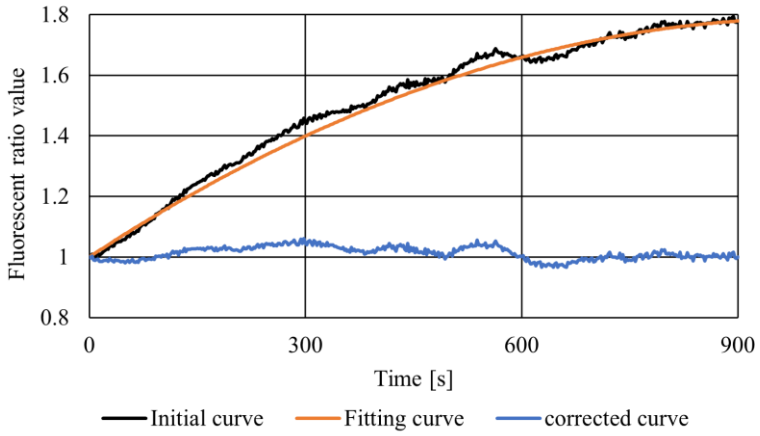

Fig.6 Example of the slope correction of the normalized fluorescent ratio value curve

To maintain a constant ratio of cell fluorescence to a background in the ROI, the ROI was set to 2.5 times the area of the cell before vibration (initial state), and the average fluorescence intensity for the image data taken under all conditions was measured (No vibration, 45 Hz vibration and 90 Hz vibration). To set the ROI with 2.5 times larger area, the width of the ROI was stretched toward the direction of the vibration (left-right direction in the figure). The 2.5-fold width was the minimum width that could enclose a fluorescent image with distortions without it protruding from the ROI under the 45 Hz and 0.2 g condition.

The temporal changes in the fluorescent ratio values of Fluo 8H and Calcein Red-Orange were affected by the different bleaching rates of the two fluorescent dyes and cellular activity signals on the order of several hours, resulting in a sustained increase or decrease in fluorescence. Therefore, the slope of the fluorescent ratio value curve was corrected. As shown in Fig.6, the slope was corrected by subtracting an approximate curve fitted by a quadratic function from the original curve. In addition, the fluorescence intensity ratio varies greatly from cell to cell, making it difficult to compare the change between cells. Therefore, in this study, the fluorescence intensity ratio was normalized to an initial value of 1 for each cell.

2.5 Indicators to evaluate cellular response characteristics and statistical analysis

Figure 7 shows the fluorescent ratio graph of the cells in the control group, which were imaged in a static state without vibration stimulation (n = 20 cells from 5 experiments). The mean value of the fluorescent ratio peak of the cells was 1.053. Therefore, the threshold value for determining the presence or absence of the cellular response was set to 1.06. The cells were judged to have responded when the fluorescent ratio value exceeded 1.06 and the condition lasted for more than 10 seconds.

In this study, the cell response rate, response intensity, and response duration indices were used to evaluate the response characteristics of the cells. The response rate is the percentage of responding cells among all cells in each cell group, the response intensity is the mean peak value of the fluorescent ratio of responding cells, and the response duration is the time the fluorescent ratio values exceeded the threshold values.

[DOI: 10.1299/jbse.21-00294]

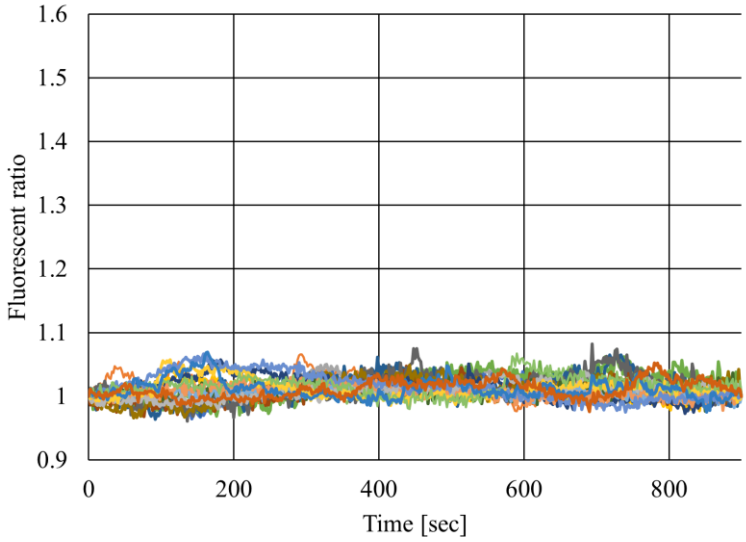

Fig.7 Time course change in normalized fluorescent ratio values in the non-vibration group (n = 20) (Control group).

In the statistical analysis, Fisher's exact probability test was used to test the cell response rate. For the response intensity and response duration, we first tested whether each indicator follows a normal distribution using the Shapiro Wilk test. Because all indices in this experiment follow a normal distribution, we tested for statistically significant differences between the groups using Welch's t-test. All statistical analyses were performed with EZR (Saitama Medical Center, Jichi Medical University, Saitama, Japan), a graphical user interface for R (The R Foundation for Statistical Computing, Vienna, Austria). More precisely, it is a modified version of R commander designed to add statistical functions frequently used in biostatistics (Kanda, 2013).

3. Results

3.1 Driving test of the device

Figure 8 shows the imaging position during the driving test. During imaging, 2 ml of water was added to the glass bottom dish to match the mass with the actual cell response observation. The image was taken at the edge of the hole on the bottom of the dish. The area enclosed by the light blue rectangle in the figure is the actual imaging area. Figure 9 plots the line profile of the red line indicated in Figure 8 on the vertical axis with time on the horizontal axis. The line profile was binarized to clarify the position of the hole edges. The number of peaks and troughs in the unit time of the graph confirmed that the edge was moving back and forth at 45 Hz and 90 Hz. The amplitude of the displacement of the

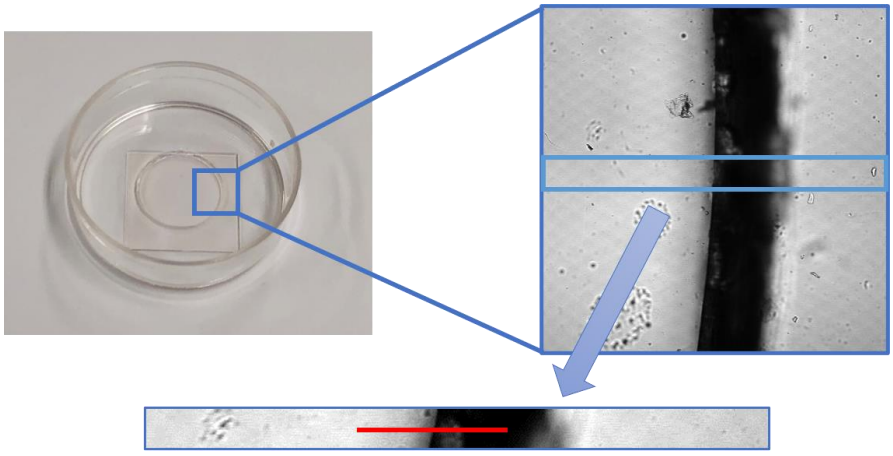

Fig.8 Imaging position in the driving test. The actual imaging area is enclosed by the light blue rectangle and the line profile on the red line is plotted on the graph.

[DOI: 10.1299/jbse.21-00294]

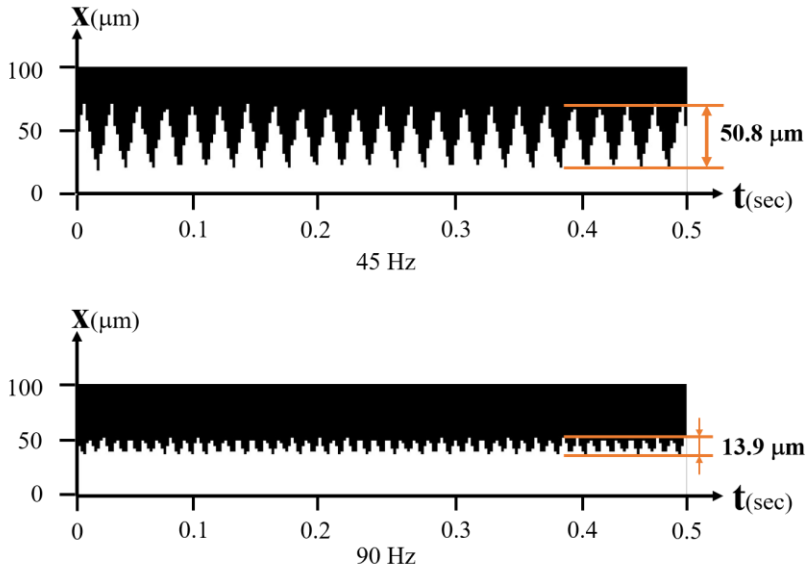

Fig.9 Graph of the line the profiles in a drive test plotted against the passage of time.

edge was 50.8 μm when the device was driven at 45 Hz, and 13.9 μm at 90 Hz. These amplitudes corresponded to the target acceleration amplitude of 0.2 g. On another day, the displacement amplitudes were 52.9 μm and 12.3 μm, respectively. The variability in the re-measured values corresponds to 1 or 2 pixels of the acquired image and can be attributed to image measurement error. This measurement error corresponds to approximately 0.02 g or 0.01 g in terms of acceleration amplitude (45 Hz, 90 Hz). Therefore, the accuracy of the vibration intensity guaranteed by the developed device is approximately 0.02 g. The driving tests confirmed that the developed device provided the desired frequency and acceleration amplitude to the glass bottom dish.

3.2 Characteristics of the intracellular calcium signaling response to vibration stimuli

Figure 10 and Figure 11 show the temporal changes in the fluorescence intensity ratio of osteoblasts subjected to 45 Hz and 90 Hz vibration stimulation, respectively. Table 1 shows the percentage of responded cells in each group. No cells in the non-vibration group were judged to be responsive. In contrast, 75 % (15/20 cells) and 45 % (9/20 cells) of the cells in the 45 Hz and 90 Hz vibration groups, respectively, were responsive. In terms of the percentage of cells that responded, the 45 Hz vibration group showed a greater response rate, though not significantly different than the 90 Hz vibration group (p = 0.105).

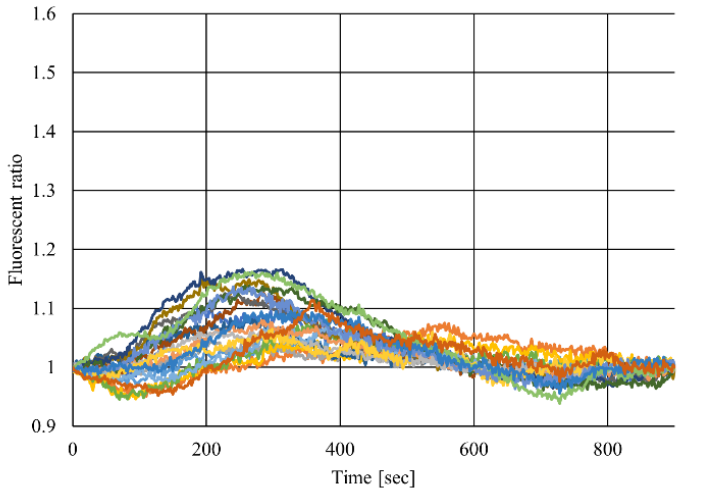

Fig.10 Time course change in normalized fluorescent ratio values in 45 Hz vibration group (n = 20 from 4 times experiments)

[DOI: 10.1299/jbse.21-00294]

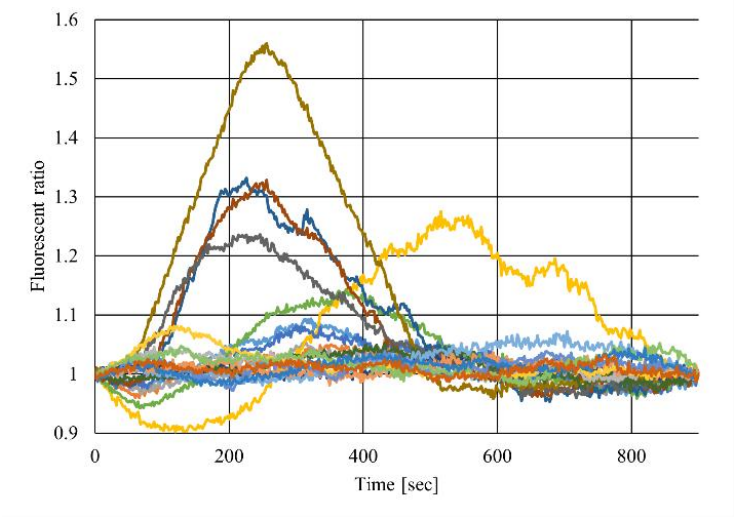

Fig11 Time course change in normalized fluorescent ratio values in 90 Hz vibration group (n = 20 from 4 times experiments)

Table 1 Percentage of responded cells

	Percentage of responded cells
Non vibration	0 % (0 / 20 cells)
45 Hz vibration	75 % (15 / 20 cells)
90 Hz vibration	45 % (9 / 20 cells)

Figure 12 and Figure 13 show the mean values of response intensity and response duration for the 45 Hz and 90 Hz vibration groups, respectively. In the 45 Hz group, the mean value of response intensity was 1.11±0.03, and 1.24±0.16 for the 90 Hz group. The response durations were 185±111 (seconds) in the 45 Hz group and, 282±147 in the 90 Hz group. The comparison of the response intensity showed that the 90 Hz vibration group had greater response intensity, and there was a statistically significant difference between this group and the 45 Hz group. There was a tendency for the 90 Hz vibration group to have a longer response duration, although it was not significantly different than the 45 Hz group (p = 0.107).

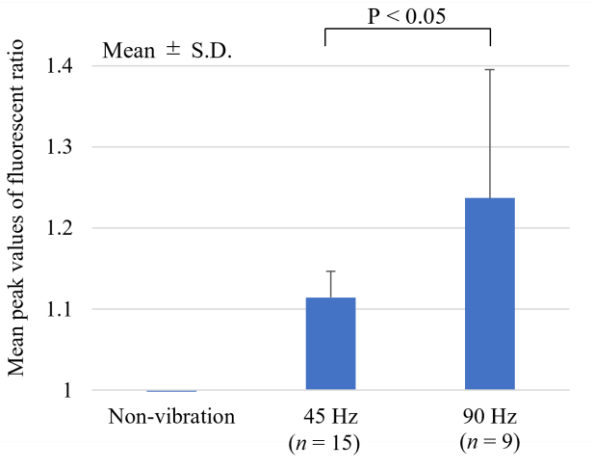

Fig.12 Comparison of the response intensity between each cell group. The response intensity of the 90 Hz vibration group was greater than that of the 45 Hz vibration group, and the difference was statistically significant.

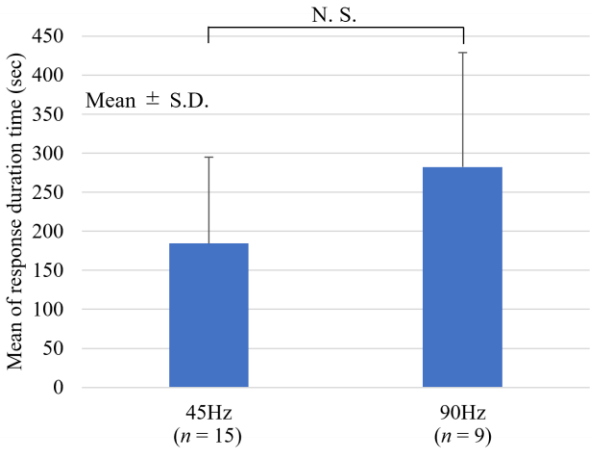

Fig.13 Comparison of the response durations between the different cell groups. The 90 Hz vibration group tended to have a longer response duration than the 45 Hz vibration group; however, the difference was not statistically significant (p = 0.107).

[DOI: 10.1299/jbse.21-00294]

4. Discussion

A frequency of 15 Hz to 90 Hz and an acceleration amplitude of 0.1 g to 0.3 g are LMHF vibration stimulus conditions in studies using model animals. We designed a device to observe the response of osteoblasts *in situ* under the vibration conditions employed in previous studies. The device is capable of reproducibly and accurately applying LMHF vibration stimuli with an acceleration amplitude of 0.2 g to a glass bottom dish at frequencies of 45 Hz and 90 Hz. In addition, it is possible to generate and deliver 0.2 g vibration stimuli up to 135 Hz for a higher frequency range (data not shown). Alternatively, on the low frequency side, the acceleration amplitude of 0.2 g was not achieved for frequencies of 15 Hz and 30 Hz. The physical amplitude required to generate the same acceleration amplitude becomes larger at lower frequencies. Because the piezoelectric actuator used in the developed device has a mechanism that increases the stroke by converting the expansion and contraction of the piezoelectric actuator into a pivoting motion, the displacement in the direction perpendicular to the main motion axis also increases as the stroke increases, which results in an increase in the movement resistance of the linear slider. Ripples were also observed on the surface of the buffer solution in the glass bottom dish when 0.1 g of vibration was generated at 15 Hz and 30 Hz. This may cause a large disturbance of the buffer solution, resulting in mechanical stimulation of the cells other than vibration such as fluid shear. For these reasons, we decided not to use the device for vibration stimuli at frequencies of 15 or 30 Hz, which is a limitation of this device.

A confocal laser scanning fluorescence microscope was used to measure the changes in intracellular calcium ion concentration. Because of the imaging principle of the scanning microscope, the cells under observation are subjected to periodic distortions when vibration is applied. In this study, we introduced a large ROI, including the cell shape distortion, and measured the average fluorescence intensity in the ROI. To keep the ratio of the cell body to background in the ROI constant between the 45 Hz and 90 Hz groups, the ROI was set to an area 2.5 times larger than the area of the cell body at rest. This means that even if the fluorescence intensity of the cell body changes, it is averaged by the background intensity value (constant value) in the ROI, resulting in a decrease in sensitivity to capture the response. Furthermore, because of the distortion of the fluorescence images, it is not possible to evaluate the calcium signaling response at the intracellular microstructure level. However, the origin of the calcium signaling response in the cell is of great interest because it may provide very powerful insight into the mechanotransduction mechanism of LMHF vibration stimuli. This problem could be solved by using a high-speed camera imaging system for ratiometric observation (likely with two cameras), or by constructing an image processing software algorithm that can extract only cell bodies and update the ROI for each temporal observation image. However, this would be limited by cost and resources required for image processing of the acquired data.

We would like to discuss one more limitation in our experimental system. As shown in Figures 10 and 11, the fluorescent ratio values of some cells dropped below 0 after starting the vibration stimulation. This is considered an artifact of the slope correction of the curve of the time-course change in the fluorescent ratio value. The slope of the fluorescent ratio curve is corrected mainly to reduce the effect caused by the difference in the bleaching rate of Fluo 8H and Calcein Red-Orange. Without slope correction, it is not possible to define a threshold for determining the presence or absence of a cellular response. However, because of the artifacts caused by the slope correction, the characteristics of the calcium signaling response of the cell may be overlooked. The ratiometry method was originally used to correct the effect of out-of-focus images because of vibration; however, the slope of the fluorescent ratio curve needed to be corrected. Because the out-of-focus effect was not as large as expected, we may need to consider switching to an experimental system using only Fluo 8H to eliminate the artifacts caused by the slope correction of the fluorescent ratio curve.

We were able to observe the calcium signaling response of osteoblasts stimulated by LMHF vibration at the single cell level *in situ* using the developed device. The intracellular calcium ion concentration of osteoblasts in response to the LMHF vibration stimulation increased within tens of seconds after the stimulation. This transient increase in intracellular calcium ion concentration returned to the pre-stimulus level within a few minutes. This change may indicate that calcium signaling is regulated by the ability to maintain intracellular calcium ion concentration homeostasis even after continuous LMHF vibration stimulation for 15 minutes, or it may represent the acclimation effect of cells to LMHF oscillatory stimulation. Previous studies using animal models reported that vibration stimulation with a pause was more effective in promoting bone formation than continuous vibration stimulation (Xie, et al., 2006; Matsumoto, et al., 2008). Our results may provide a cellular level interpretation of reports that inserting a resting phase more effectively promotes bone formation. What kind of response is produced by continued application of the LMHF vibration stimulation after the

[DOI: 10.1299/jbse.21-00294]

transient calcium signaling response subsides? It is necessary to conduct an *in situ* observation for a longer period of time. Our experimental system may provide useful insights into the length and frequency of more effective rest periods.

A statistically significant difference was found in the calcium signaling response intensity of osteoblasts at different LMHF vibration stimulation frequencies. In addition to the mean peak values, the graph of the time-course change in fluorescent ratio values shows that the calcium signal response was stronger in the 90 Hz vibration group. Alternatively, there were a certain number of cells with the same response intensity as that of the 45 Hz vibration group even when the 90 Hz stimulus was applied. Although there was no statistically significant difference in the response rate and response duration of the cells, the response rate was greater in the 45 Hz group, and the response duration tended to be longer in the 90 Hz group. It is clear that the characteristics of the calcium signaling response of osteoblasts to LMHF vibration stimulation can vary depending on the vibration conditions. Future studies using the developed device to evaluate the calcium signaling response characteristics of osteoblasts under more vibration conditions may yield results that show, for example, an increase in cell response in a specific frequency range. If we can identify such vibration conditions, we can expect to gain important insight into the unknown cellular mechanisms that sense LMHF vibration.

5. Conclusion

We developed a device for *in situ* microscopic observation of osteoblast response to LMHF vibration stimulation. The developed device accurately and reproducibly applied LMHF vibration stimuli with an acceleration amplitude of 0.2 g at frequencies of 45 Hz and 90 Hz to a glass bottom dish. The LMHF vibration stimulation was applied to osteoblasts, and the calcium signal response to the stimulation was observed fluorescently. The results showed that it is possible to evaluate the calcium signaling response of osteoblasts to LMHF vibration stimulation at the single cell level. The calcium signaling response of osteoblasts showed a stronger response intensity at a vibration frequency of 90 Hz. Although there was no statistically significant difference, the cell response rate showed a higher percentage for the 45 Hz vibration, and the response duration tended to be longer for the 90 Hz vibration. This device will enable detailed observation of the response characteristics of osteoblasts to LMHF vibration, and it is expected to provide insights into the currently unexplored mechanosensory mechanisms of osteoblasts to LMHF vibration stimuli.

Acknowledgment

This study was supported by Support Center for Advanced Medical Sciences, Tokushima University Graduate School of Biomedical Sciences. This study was partly supported by JSPS KAKENHI Grant Number 20K12601. We thank Ashleigh Cooper, PhD, from Edanz (https://jp.edanz.com/ac) for editing a draft of this manuscript.

References

Fritton, S. P., McLeod, K. J., Rubin, C. T., Quantifying the strain history of bone: spatial uniformity and self-similarity of low-magnitude strains, Journal of Biomechanics, Vol.33, No.3, (2000), pp.317-325.

Godin, L. M., Suzuki, S., Jacobs, C. R., Donahue, H. J. and Donahue, S. W., Mechanically induced intracellular calcium waves in osteoblasts demonstrate calcium fingerprints in bone cell mechanotracsduction, Biomechanics and Modeling in Mechanobiology, Vol.6, No.6, (2007), pp.391-398.

Huo, B., Lu, X. L., Hung, C. T., Costa, K. D., Xu, Q., Whitesides, G. M. and Guo, X. E., Fluid flow induced calcium response in bone cell network, Cellular and Molecular Bioengineering, Vol.1, No.1, (2008), pp.58-66.

Hwang, S. J., Lublinsky, S., Seo, Y.K., Kim, I.S., Judex, S., Extremely small-magnitude accelerations enhance bone regeneration: a preliminary study, Clinical Orthopaedics and Related Research, Vol.467, No.4, (2009), pp.1083-1091.

Judex, S., Lei, X., Han, D., Rubin, C., Low-magnitude mechanical signals that stimulate bone formation in the ovariectomized rat are dependent on the applied frequency but not on the strain magnitude, Journal of Biomechanics, Vol.40, No.6, (2007), pp.1333-1339.

Kanda, Y., Investigation of the freely available easy-to-use software 'EZR' for medical statistics, Bone Marrow Transplantation, Vol.48, (2013), pp.451-458.

[DOI: 10.1299/jbse.21-00294]

Leung, K. S., Shi, H.F., Cheung, W. H., Qin, L., Ng, W. K., Tam, K.F., Tang, N., Low-magnitude high-frequency vibration accelerates callus formation, mineralization, and fracture healing in rats, Journal of Orthopaedic Research, Vol.27, No.4, (2009), pp.458-465.

Levin, V.A., Jiang X., Kagan, R., Estrogen therapy for osteoporosis in the modern era. Osteoporos International, Vol.29, No.5, (2018), pp.1049-1055.

Lindsay, R. and Tohme, J. F., Estrogen treatment of patients with established postmenopausal osteoporosis, Obstetrics and Gynecology, Vol.76, No.2, (1990), pp.290-295.

Lu, X. L., Huo, B., Chiang, V. and Guo, X. E., Osteocytic netword is more responsive in calcium signaling than osteoblastic network under fluid flow, Journal of Bone and Mineral Research, Vol.27, No.3, (2012), pp.563-574.

Matsumoto, N. H., Koyama, Y. and Takakuda, K., Effect of mechanical loading timeline on periosteal bone formation, Journal of Biomechanical Science and Engineering, Vol.3, No.2, (2008), pp.176-187.

Rubin, C., Recker, R., Cullen, D., Ryaby, J., McCabe, J., McLeod, K., Prevention of postmenopausal bone loss by a low-magnitude, high-frequency mechanical stimuli: a clinical trial assessing compliance, efficacy, and safety, Journal of Bone Mineral Research, Vol.19, No.3, (2004), pp.343-351.

Tezval, M., Biblis, M., Sehmisch, S., Schmelz, U., Kolios, L., Rack, T., Stuermer, K. M., Stuermer, E. K., Improvement of femoral bone quality after low-magnitude, high-frequency mechanical stimulation in the ovariectomized rat as an osteopenia model, Calcified Tissue International, Vol.88, No.1, (2010), pp.33-40.

Xie, L., Jacobson, J. M., Choi, E. S., Busa, B., Donahue, L. R., Miller, L. M., Rubin, C.T., Judex, S., Low-level mechanical vibrations can influence bone resorption and bone formation in the growing skeleton, Bone, Vol.39, No.5, (2006), pp.1059-1066.

[DOI: 10.1299/jbse.21-00294]